2009 6th International Multi-Conference on Systems, Signals and Devices

NONSMOOTH PITCHFORK BIFURCATION IN A DC-DC CONVERTER: COEXISTING ATTRACTORS AND INTERMITTENCY

Abdelali El Aroudi[1], *Vanessa Moreno-Font*[2], *and Luis Benadero*[2]

[1]Departament d'Enginyeria Electrònica, Elèctrica i Automàtica (DEEEA),
Universitat Rovira i Virgili Tarragona, Spain,
e-mail: abdelali.elaroudi@urv.cat
[2]Departament de Fìsica Aplicada,
Universitat Politècnica de Catalunya, Barcelona, Spain,
(luis,vanessa)@fa.upc.edu

ABSTRACT

In this paper we deal with the analysis of nonlinear dynamical behavior of a single inductor two inputs two outputs (SITITO) power electronics DC-DC converter. The system can be used to regulate generally two outputs (one positive and one negative). Under certain operating conditions, the switching model can be approximated by a one dimensional piecewise constant vector field and, as a consequence, the corresponding map is piecewise linear (PWL). This model is derived and then it is used to study a nonsmooth pitchfork bifurcation in the system. Coexistence of attractors are detected by using the same model. Intermittent chaotic behavior is also addressed. Analytical results are confirmed by one dimensional and two-dimensional bifurcation diagrams.

Keywords: single inductor, DC-DC converters, nonlinear dynamics, bifurcations, chaos, pitchfork, nonsmooth.

1. INTRODUCTION

Switching power converters are widely used in the power management area, due to their potential of high efficiency, low cost and small size [1]. In most of the applications, these systems are used in situations where there is a need to stabilize an output voltage to a desired constant value.

The demand for portable equipments in modern vehicles such mobile phones, MP3 players, PDAs, GPS, has grown significantly during the last few years. The portable equipments usually include a variety of loads such as LCD displays, memories, microprocessors, Universal Series Bus (USB) and Hard Disk Drives (HDD). These loads require different operating voltages and load currents and are powered by the rechargeable batteries through DC-DC converters. To make longer the system run life and smaller its size, more and more system designers are focusing on improving the system power conversion efficiency with advanced power converters topologies. The traditional solution of using independent converters one for each of the outputs has the shortcomings of higher number of switches and magnetics components. Besides this option and other dual DC-DC converter configurations [2]-[9], single inductor multiple inputs multiple output (SIMIMO) DC-DC converters are, in general, convenient solutions for these low power applications.

Nowadays, there are many works dealing with nonlinear behavior in elementary stand alone [10] and other more complex power electronics circuits such as paralleled DC-DC converters [11], multi-cell and multi-level converters [12]-[14] and also for an example of single inductor two input two output (SITITO) converters [7].

In this paper, more insights into the modeling and analysis of a SITITO interleaved converter is presented. After giving the switched model, a systematic approach is described to obtain a simple PWL map that can be used to predict accurately the fast scale (switching) dynamics of the system. The model will be used to get some analytical conditions for stability of the system and for optimizing its performances.

The rest of the paper is organized as follows. Section II deals with the description of the SITITO DC-DC converter and the basis for the interleaving control circuit is presented. Then in Section III, the mathematical model is given. Under the assumption of perfect output regulation, the general PWL map is derived. Section IV will deal with stability analysis by using this PWL map. We will use the derived map to get some analytical expressions for stability conditions and to draw some bifurcation curves of the system. Section V includes some numerical simulations from the PWL map and one-dimensional and two-dimensional bifurcation diagrams of the system by using the PWL map. Basins of attraction are addressed in section VI. Finally, some conclusions are given in the last section.

This work was partially supported by the Spanish MED under grant TEC-2004-05608-C02-01 and TEC-2007-67988-C02-01. EU FENDER funds is also acknowledged.

978-1-4244-4346-8/09/$25.00 ©2009 IEEE

2. SINGLE INDUCTOR TITO DC-DC REGULATOR

2.1. Power stage circuit

The schematic diagram in Figure 1 shows a DC-DC converter with a single inductor for two outputs V_P and V_N with opposite polarity. The voltages of both loads are regulated from the power source V_{in} by generating a sequence of command signals driving switches S_A and S_B.

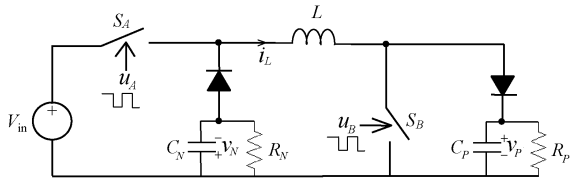

Figure 1. Schematic diagram of a single inductor DC-DC converter with positive v_P and negative v_N output voltages.

2.2. Pulse Width Modulation Strategy with Interleaving

One control strategy for the SITITO topology of Figure 1, which is based on an interleaved current mode control, was proposed in [9] (See Figure 2). This control strategy works

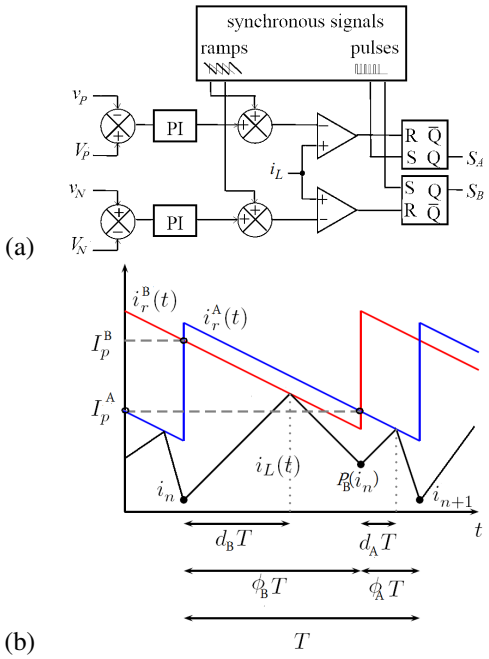

Figure 2. Control strategy of single inductor two outputs converter of Figure 1 based on interleaved pulse width modulation. The feedback current is i_L. Control signals for the SITITO interleaved DC-DC converter

as follows: the two ramp reference signals, which are associated to each of the channels, are are phase-shifted (interleaved) so that in the steady state regime, a sequence of time intervals, once per channel, will be produced. In this way, the ramp reference signal v_r^j ($j \in \{A, B\}$) corresponding to channel j is shifted by a phase shift ϕ_j. Based on current mode control, the general idea is to obtain a current reference v_r^j for each channel (output). These signals are to be compared to the inductor current i_L. Figure 2-b, shows the relevant control signals and parameters of the system.

3. CLOSED LOOP MATHEMATICAL MODELING

3.1. Switched model for the SITITO converter

The switched model gives the set of five equations for the different configurations of the system. It contains the binary signals u_A and u_B and the instantaneous state variables. This model can be easily obtained by applying standard Kirchhoff's voltage law to the circuit [7]:

$$\frac{dv_P}{dt} = \frac{1}{C_P}\left(i_L(1-u_B) - \frac{v_P}{R_P}\right) \tag{1}$$

$$\frac{dv_N}{dt} = \frac{1}{C_N}\left(-i_L(1-u_A) - \frac{v_N}{R_N}\right) \tag{2}$$

$$\frac{ds_P}{dt} = \frac{1}{\tau_P}(V_P - v_P) \tag{3}$$

$$\frac{ds_N}{dt} = \frac{1}{\tau_N}(v_N - V_N) \tag{4}$$

$$\frac{di_L}{dt} = \frac{1}{L}(u_B - 1)v_P + \frac{1}{L}(1-u_A)v_N + \frac{1}{L}(-r_L i_L + V_{\text{in}}u_A) \tag{5}$$

where v_P is the voltage across the capacitor C_P, v_N is the voltage across the capacitor C_N, i_L is the current through the inductor L whose equivalent series resistance is r_L. s_P and s_N are the integral variables and τ_P and τ_N are the time constants in the corresponding PI integrators. u_A and u_B are the driving binary signal which are 1 if the corresponding switch is ON and 0 if the switch is OFF. v_r^A and v_r^B are the reference currents that can be expressed as:

$$v_r^A(t) = g_P(V_P - v_P + s_P) + v_{\text{ramp}}^A(t) \tag{6}$$

$$v_r^B(t) = g_N(v_N - V_N + s_N) + v_{\text{ramp}}^B(t) \tag{7}$$

where

$$v_{\text{ramp}}^A(t) = V_u - (V_u - V_l)\text{mod}\left(\frac{t}{T}, 1\right) \tag{8}$$

$$v_{\text{ramp}}^B(t) = V_u - (V_u - V_l)\text{mod}\left(\frac{t}{T} - \phi_B, 1\right) \tag{9}$$

mod$(\cdot)$ stands for the modulus function and $\phi_A = 1 - \phi_B$. The first subset of two equations (Eq. 1) refers to the dynamics of the voltage output v_P and v_N. R_P and R_N are the resistive load for both outputs. Additional subset (Eq. 3 and Eq. 4) deal with two equations for each of the integral terms s_P and s_N, being V_P and V_N the reference voltages. The last equation (Eq. 5) deals with inductor current dynamics. During each switching period, the

switch S_A (resp. S_B) is closed for a time duration $d_A T$ (resp. $d_B T$). The duty ratios d_A and d_B for each ON sub-interval, which are determined by the action of comparator, can be expressed implicitly in terms of the state variables as follows:

$$i_r^A(t) - i_L = 0 \tag{10}$$
$$i_r^B(t) - i_L = 0 \tag{11}$$

where $i_r^j(t) = v_r^j(t)/r_S$, $j \in \{A, B\}$. Obtaining d_A and d_B requires solving Eqs. (10) and (11). If these equations are not feasible, the duty cycles are saturated to their limit values 0 or 1 depending on the relation between the control signal $r_S i_L$ and the ramp signals v_r^j. The above set of five state equations is the closed switched continuous time model that can be used for computer simulations of the whole system.

3.2. Piecewise linear map

In this section we will give a one dimensional map that can capture the fast scale dynamic of the SITITO interleaved converter. Under the assumption that outputs v_P and v_N are well regulated to their desired values V_P and V_N respectively, this map is a one-dimensional map and the state variable is the discrete-time current $i_n := i_L(nT)$. This assumption was done in [8] for elementary DC-DC converters. Due to the different operating modes that the system can present (d_A and/or d_B non-saturated and saturated), the one-dimensional map has different forms. Independently on the operating mode, it can be shown that the mapping can be written in the following form:

$$P(i_n) = P_A \circ P_B(i_n) \tag{12}$$

where P_j is the local sub-mapping defined by:

$$P_j(x) = \begin{cases} x + m_{on}\phi_j T, & \text{if } d_j > \phi_j \\ x + m_{on} d_j T + m_{off}^j(\phi_j - d_j)T, & \text{if } d_j < \phi_j \end{cases} \tag{13}$$

where x is the state variable at the beginning of phase j and m_{on} and m_{off}^j are the approximated slopes of the inductor current during the ON and the OFF phases and that are given by:

$$m_{on} = \frac{V_{\text{in}} - r_L I_L}{L} \tag{14}$$
$$m_{off}^P = \frac{V_{\text{in}} - V_P - r_L I_L}{L} \tag{15}$$
$$m_{off}^N = \frac{V_N - r_L I_L}{L} \tag{16}$$

In the expressions of m_{on}, m_{off}^P and m_{off}^N the term $r_L i_L$ which appears in the inductor current state equation was approximated by $r_L I_L$. The parameter I_L is obtained by means of the averaged model and it is given by [7]:

$$I_L = \frac{V_{\text{in}}}{2r_L} + \sqrt{\frac{V_{\text{in}}^2}{4r_L^2} - \frac{1}{r_L}\left(\frac{V_P^2}{R_P} + \frac{V_N(V_N - V_{\text{in}})}{R_N}\right)} \tag{17}$$

Figure 3 shows the cobweb plot of the map P for different values of r_S. Note the richness of behavior that the map can exhibit. Namely, in Fig. 3-a and Fig. 3-e, the system has only one real fixed point. The other two fixed points are virtual. For Fig. 3-b and Fig. 3-f, the virtual fixed points become real through a non smooth pitchfork bifurcation as we will see later. In Fig. 3-c and Fig. 3-g, two attractors are coexisting, one is chaotic and the other one is a fixed point. For Fig. 3-d and Fig. 3-h, a single chaotic attractor exists after a boundary crisis.

The duty cycles d_A and d_B are obtained by assuming that the inductor current is linear during each charging phase, then, the following expressions are obtained:

$$d_A = \frac{I_p^A - i_n^A}{(m_{on} - m_r)T} \tag{18}$$
$$d_B = \frac{I_p^B - i_n^B}{(m_{on} - m_r)T} \tag{19}$$

where $i_n^B = i_n$, $i_n^A = P_B(i_n)$, I_p^A and I_p^B are respectively the value of $i_r^A(t)$ and $i_r^B(t)$ at the beginning of phases A and B, and

$$m_r = -\frac{V_U - V_L}{r_S T} \tag{20}$$

The fixed points are obtained by forcing that $i_{n+1} = i_n$. Depending on the parameters of the circuit, there can exist one (nonsaturated), or three (one unsaturated and two saturated) fixed points (see Fig. 3). The unsaturated fixed point i_d is given by the following expression:

$$\begin{aligned} i_d = I_L &+ \left(\frac{D_A^2 + D_B^2}{2} - \phi_A D_A - D_B\right) m_{on} T \\ &+ \left(D_B\left(1 - \frac{D_B}{2}\right) - \phi_B\left(\phi_A + \frac{\phi_B}{2}\right)\right) m_{off}^B T \\ &+ \left(\phi_A D_A - \frac{D_A^2}{2} - \frac{\phi_A^2}{2}\right) m_{off}^A T \end{aligned} \tag{21}$$

where the average duty cycles corresponding to each phase can be obtained from the averaged model and they are given by [9]:

$$D_A = \phi_A - \left|\frac{V_N}{R_N I_L}\right| \tag{22}$$
$$D_B = \phi_B - \left|\frac{V_P}{R_P I_L}\right| \tag{23}$$

The two other fixed points when they exist are given by:

$$\begin{aligned} i_{dA} &= I_P^2 - m_r \phi_B T + m_{off}^A \frac{m_{on} - m_r}{m_{on} - m_{off}^A} T \\ i_{dB} &= I_P^1 - (m_{on} - m_r)\left(\phi_B - \frac{m_{on}}{m_{on} - m_{off}^B}\right) T \end{aligned} \tag{24}$$

These fixed points can only exist if the derivative of the map at the nonsaturated fixed point is bigger than 1.

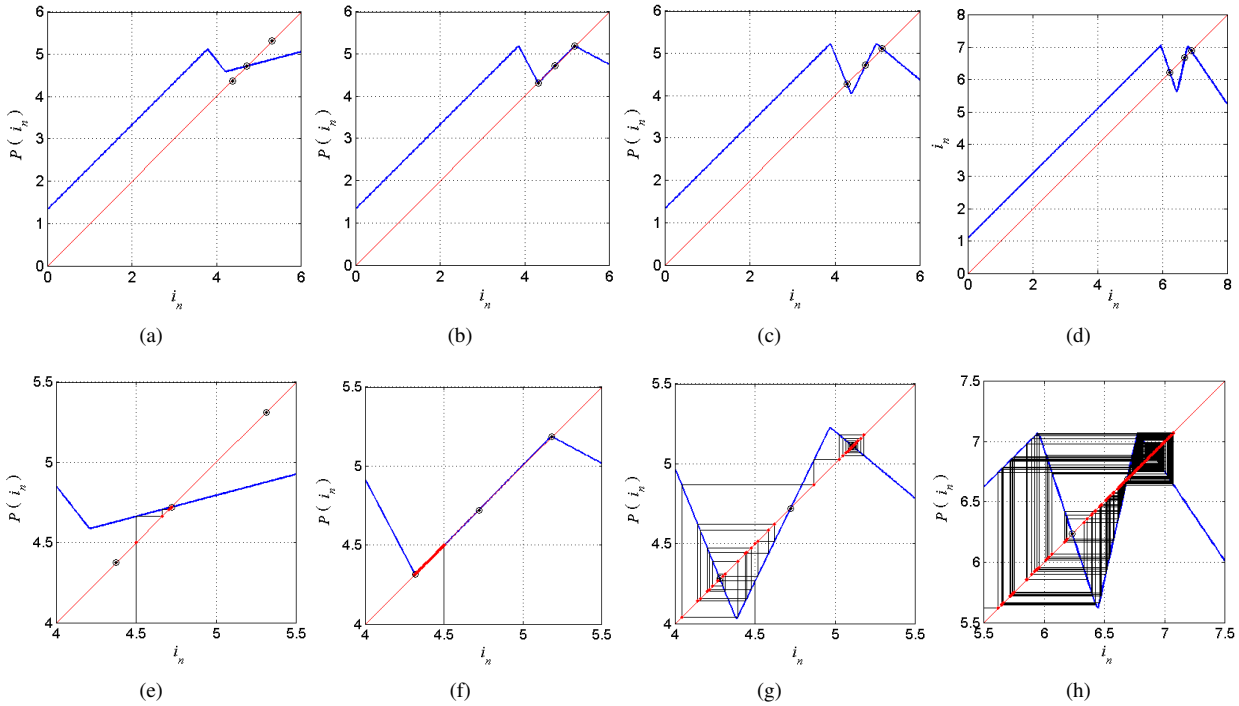

Figure 3. The form of the map P and the cobweb plot near the fixed points for different values of r_S. (a, e) $r_S = 1\,\Omega$, $V_P = 18\,V$, (b, f) $r_S = 2\,\Omega$, $V_P = 18\,V$, (c, g) $r_S = 3\,\Omega$, $V_P = 18\,V$ and (d, h) $r_S = 5\,\Omega$, $V_P = 21\,V$. (a-d) overview of the PWL map. (e-h) zoom near the fixed points.

4. NONSMOOTH PITCHFORK BIFURCATION

4.1. The stability indexes

A sufficient condition for stability of the nonsaturated fixed point is that the absolute value of the derivative λ of the map P evaluated at this fixed point is smaller than 1. It can be shown that this derivative is:

$$\lambda(i_d) = \frac{(m_{off}^P - m_r)(m_{off}^N - m_r)}{(m_{on} - m_r)^2} \tag{25}$$

If for a certain choice of parameters, this derivative becomes larger than one then, the two saturated fixed points are created (they pass from virtual to real). The derivative of the map at i_{dA}

$$\lambda(i_{dA}) = \frac{(m_{off}^P - m_r)}{(m_{on} - m_r)} \tag{26}$$

Likewise, the derivative of the map at i_{dB} is

$$\lambda(i_{dB}) = \frac{(m_{off}^N - m_r)}{(m_{on} - m_r)} \tag{27}$$

Let us define the following set of parameters:

$$\kappa = \frac{L(V_u - V_l)}{r_S T} \tag{28}$$

$$\alpha = r_L I_L - V_{\text{in}} + V_P \tag{29}$$

$$\beta = r_L I_L + V_N \tag{30}$$

$$\gamma = r_L I_L - V_{\text{in}} \tag{31}$$

With these definitions the stability indexes λ become

$$\begin{aligned} \lambda(i_d) &= \frac{(\kappa - \alpha)(\kappa - \beta)}{(\kappa - \gamma)^2} \\ \lambda(i_{dA}) &= \frac{\kappa - \alpha}{\kappa - \gamma} \\ \lambda(i_{dB}) &= \frac{\kappa - \beta}{\kappa - \gamma} \end{aligned} \tag{32}$$

It can be observed that as $\lambda(i_d) = \lambda(i_{dA})\lambda(i_{dB})$ and that after a pitchfork bifurcation $\lambda(i_d) > 1$, it is always true that $|\lambda(i_{dA})| > 1$ or $|\lambda(i_{dB})| > 1$. This means that the saturated fixed points cannot be both stable. This characteristic is different from the case of a smooth pitchfork bifurcation where the stability of the created fixed points is symmetric.

4.2. Nonsmooth pitchfork bifurcation

If for a certain choice of parameter values one has $\lambda(i_d) = 1$ and $\lambda(i_{dA}) < 0$ and $\lambda(i_{dB}) < 0$, then a nonsmooth pitchfork bifurcation will occur. The critical value of r_S for which this bifurcation occurs is given by the expression:

$$r_{S,cri} = \frac{L(V_u - V_l)(V_{in} + V_P - V_N)}{T(V_N(V_{in} - V_P) + r_L I_L(V_{in} + V_P - V_N) - V_{in}^2)} \tag{33}$$

This expression will be plotted later together with the 2-D numerically obtained bifurcation diagram.

Table 1. Parameter values used in numerical simulations.

Parameter	Value	Parameter	Value
V_{in}	$12\,V$	V_l	0
L	$640\,\mu H$	V_u	1
r_L	$0.7\,\Omega$	V_P	$+18\,V$
R_N	$33\,\Omega$	V_N	$-22\,V$
R_P	$16.5\,\Omega$	f_s	$10\,kHz$
r_S	varying	$\phi_A = \phi_B$	$\frac{1}{2}$

5. BIFURCATION BEHAVIOR FROM NUMERICAL SIMULATION

Let us consider the circuit of Figure 1 with the control scheme of Figure 2. Let us consider also the values of parameters shown in Table 1. The bifurcation parameters used here are the current gain sensor r_S and the reference voltage for the positive output channel V_P. The bifurcation parameter r_S is varied in the range (1, 5) Ω and V_P is varied in the range (1, 21) V. The 2-D bifurcation diagram is shown in Fig. 4. In this figure, the period of the orbit was color coded. Only five colors were used to determine the different periodic modes that the system can present. Using more colors does not change the results because the system does not present stable periodic orbit with period bigger than four. Yellow color represent the useful stable zone (nonsaturated fixed point i_d). Brown color corresponds to the the saturated fixed point i_{dA}. Zones of higher periods and chaotic behavior are also shown as parameters r_S and V_P vary. Their period are labeled in the same diagram. One can observe that there exists a period doubling region for low values of V_P and pitchfork bifurcation region for high values of V_P. These regions are also labeled in the same figure. The period doubling region is studied by the authors in a separate paper. Here the study is limited to the pitchfork bifurcation region. In the coexistence region, a chaotic attractor coexists with the saturated fixed point i_{dA}.

Figure 5 shows the one dimensional bifurcation diagram. The fixed points are also plotted in the same figure. We can see clearly that the branches of the saturated fixed points, after the nonsaturated fixed point becomes unstable, form a shape like a pitchfork bifurcation. However, this is a nonsmooth bifurcation and as a consequence the created fixed points have not the same stability. As a result, instead of coexisting two stable fixed points after the bifurcation, here a chaotic attractor coexists with a stable fixed point. The size of chaotic attractor increases between $r_S = 2\,\Omega$ and $r_S = 3.75\,\Omega$ when this attractor undergoes a boundary crisis (the attractor collides with i_d which is a boundary between the basins of attraction) and disappears. Between $r_S = 3.75\,\Omega$ and $r_S = 5\,\Omega$ only the saturated fixed point attractor exists and the basin of attraction of the chaotic attractor becomes null. In this case, the basin of attraction of the fixed point is the entire domain of definition of the PWL map.

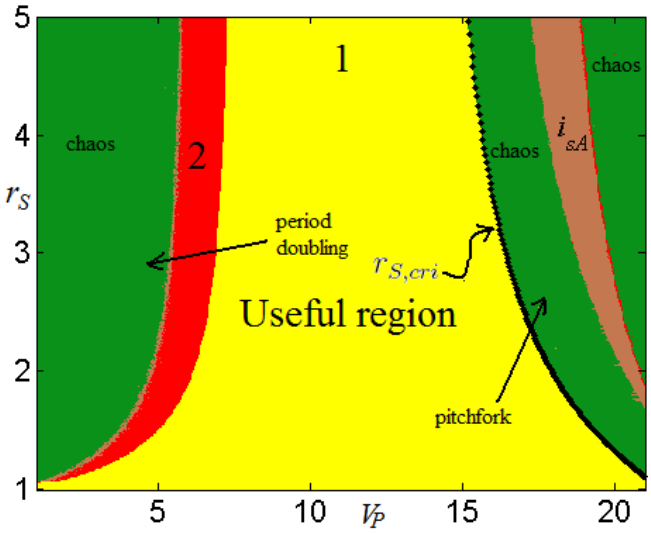

Figure 4. 2-D bifurcation diagram of the map P taking r_S and V_P as bifurcation parameters. The diagram is plotted starting from an initial condition near the average value of inductor current I_L.

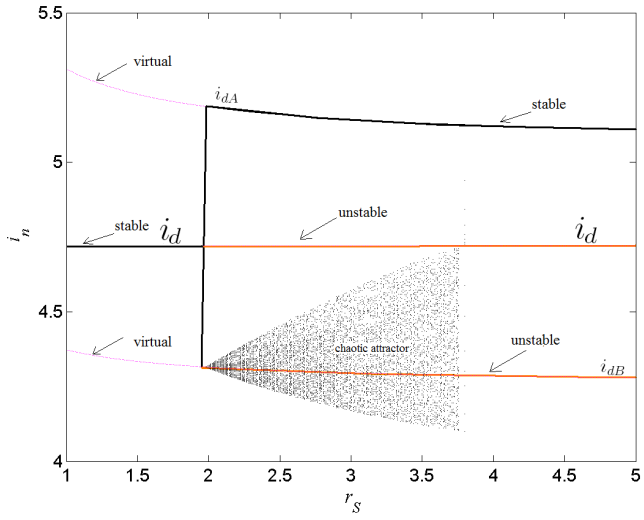

Figure 5. 1-D bifurcation diagram taking r_S as bifurcation parameter. The diagram is plotted starting from different initial conditions in order to uncover the possible coexisting attractors. The fixed points and their stability are also shown.

5.1. Coexisting period-1 orbit and chaotic attractor: $\lambda(i_{dA}) < -1$ and $-1 < \lambda(i_{dB}) < 0$

As in the case of a smooth pitchfork, two fixed points are created and, depending on their eigenvalues, we can have the possibility of two attractors for the same parameter values. The basin of attraction, which is defined as the set of points in the state space such that initial conditions chosen in this set dynamically evolve to an attractor, can be obtained by sweeping the initial condition in a certain interval. These sets can be obtained by numerical simulations. The evolution of the basins of attraction in terms of the bifurcation parameter r_S is shown in Figure 6. The boundaries between different basins of attraction are dif-

ferent unstable periodic orbits with different periodicity. The expressions of these unstable orbits can be obtained in closed form but they hold too much space and they are not given here. Initials conditions selected in the white zones will make the system to evolve to the stable non-saturated 1-periodic orbit. Initials conditions selected in the gray zones will drive the system to the stable saturated 1-periodic orbit i_{dA} while those selected in the black zones will drive the system to the chaotic attractor.

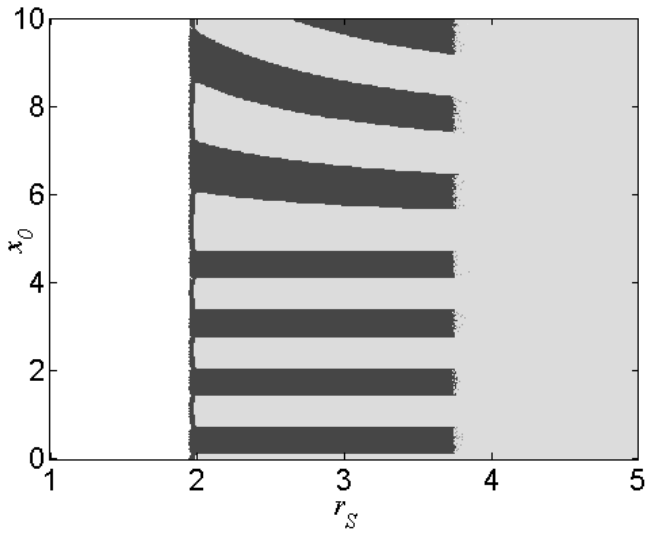

Figure 6. Evolution of the basins of attraction in term of the bifurcation parameter r_S.

5.2. Intermittent chaotic behavior: $\lambda(i_{dA}) < -1$ and $\lambda(i_{dB}) < -1$

If both saturated fixed points exist and are unstable ($\lambda(i_{dA}) < -1$ and $\lambda(i_{dB}) < -1$), then a chaotic behavior is possible. The size of the attractor is larger for smaller values of $\lambda(i_{dB})$. When the attractor collides with the nonsaturated fixed point, its size is suddenly enlarged and the attractor goes near the fixed point i_{dB} which is also a repeller point and again the trajectory moves to the fixed point i_{dA} region. This moving from one side of the nonsaturated fixed point to another gives rise to intermittent behavior as shown in Fig. 7

6. CONCLUSIONS

In this paper a single inductor two inputs two outputs (SITITO) DC-DC converter with a power stage configuration under current mode control and interleaving is studied. Its dynamics is described by a nonlinear modeling approach. An expression for a simple PWL map is derived to obtain accurate information about the dynamics of the system. This map can predict many nonlinear behaviors such as bifurcations, chaos, coexisting attractors and the associated hysteresis phenomenon and intermittent behavior. A nonsmooth pitchfork bifurcation is detected and analyzed

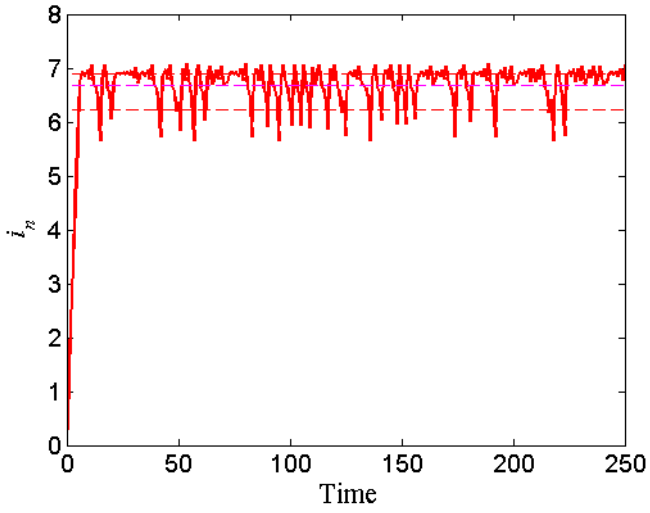

Figure 7. Intermittent behavior of the map for $r_S = 5\,\Omega$ and $V_P = 21\,V$.

for the system. Closed form expressions for the critical parameter are given in suitable design parameter space. Numerical simulations confirm the theoretical predictions.

7. REFERENCES

[1] R. W. Erickson and D. Maksimovic, *Fundamentals of Power Electronics*, Springer, 2001.

[2] I. Dénes and I. Nagy, “Two models for the dynamic behaviour of a dual-channel buck and boost DC-DC converter," *Electromotion 2003*, vol. 10, no. 4, pp. 556-561, 2003.

[3] H. P. Le, C. S. Chae, K. C. Lee, S. W. Wang and G. H. A Cho, “Single-inductor switching DC-DC converter with five outputs and ordered power-distributive control," *IEEE Journal of Solid-State Circuits*, vol. 42, no. 12, pp. 2706-2714, 2007.

[4] J. Hamar and I. Nagy, “Asymmetrical operation of dual channel resonant DC-DC converters," *IEEE Transactions on Power Electronics*, vol. 18, no. 1, pp. 83-94, 2003.

[5] R. Barabás, B. Buti, J. Hamar, I. Nagy, “Control Characteristics, Simulation and Test Results of a Dual Channel DC-DC Converter Family," *Power Electronics Electrical Drives Automation and Motion Conference*, SPEEDAM04, 16-18 June, Capri, Italy, 2004.

[6] Y. Xi and P.K. Jain, “A Forward Converter Topology with independent and precisely regulated Multiple Outputs," *IEEE Transactions on Power Electronics*, vol. 18, no. 2, pp. 648-658, 2003.

[7] L. Benadero, R. Giral, A. El Aroudi and J. Calvente, “Stability analysis of a single inductor dual switching

DC-DC converter," *Mathematics and Computers in Simulation*, vol. 71, no .4, pp. 256-269, 2006.

[8] T. Kabe, T. Saito, H. Torikai, "Analysis of Piecewise Constant Models of Power Converters", *International Symposium on Nonlinear Theory and its Applications,* Fukuoka 2004.

[9] L. Benadero, V. Moreno-Font, A. El Aroudi and R. Giral, "Single Inductor Multiple Outputs Interleaved Converters Operating in CCM," EPE-PEMC, Poznan, Poland 2008.

[10] A. El Aroudi, M. Debbat, G. Olivar, L. Benadero, E. Toribio and R. Giral, "Bifurcations in DC-DC Switching Converters Review of Methods and Applications," *International Journal of Bifurcation and Chaos*, vol. 15, vo 5, pp. 1549-1578, 2005.

[11] H. H. C. Iu and C. K. Tse, "Bifurcation behavior in parallel-connected buck converters," *IEEE Transactions on Circuits and Systems I: Fundamental Theory and Applications*, vol. 48, no. 2, pp. 233-240, 2000.

[12] A. El Aroudi, M. Debbat and L. Martinez-Salamero, "Poincaré Maps Modelling and Loal Orbital Stability Analysis of Discontinuous Piecewise Affine Periodically Driven Systems," *Nonlinear Dynamics*, vol. 50, no. 3, pp. 431-445, 2007.

[13] B. Robert and A. El Aroudi, "Discrete Time Model of a Multi-Cell DC/DC Converter: Non Linear Approach," *Mathematics and Computers in Simulation*, vol. 71, no. 4, pp. 310-319, 2006.

[14] A. El Aroudi, B. G. M. Robert, A. Cid-Pastor, and L. Martínez-Salamero, "Modelling and Design Rules of a Two-Cell Buck Converter Under a Digital Controller," *IEEE Transactions on Power Electronics,* vol. 23, no. 2, pp. 859-870, March 2008.